



Using Neutrinos to Monitor Nuclear Reactors: the Angra Neutrino Experiment, Simulation and Detector Status

J. C. Anjos^{a,*}, T. Abrahão^a, T. A. Alvarenga^b, L. P. Andrade^c, G. Azzi^a, A. S. Cerqueira^b, P. Chimenti^d, J. A. Costa^b, T. I. Dornelas^b, P. C. M. A. Farias^e, F. França^a, L. F. G. Gonzalez^e, G. P. Guedes^f, E. Kemp^e, H. P. Lima Jr^a, R. Machado^a, R. A. Nobrega^b, I. M. Pepe^g, A. L. M. Reis^c, D. B. S. Ribeiro^g, O. B. Rodrigues^e, L. M. Santos^e, S. M. V. Santos^c, E. F. Simas Filho^g, M. J. N. Souza^h, G. A. Valdivieso^c, S. Wagner^a

^aCentro Brasileiro de Pesquisas Físicas, CBPF, Rio de Janeiro-RJ, CEP22290-180, Brazil

^bUniversidade Federal de Juiz de Fora, UFJF, Juiz de Fora-MG, Brazil

^cUniversidade Federal de Alfenas, UNIFAL-MG, Poços de Caldas-MG, Brazil

^dUniversidade Federal do ABC, UFABC, Santo André-SP, Brazil

^eUniversidade Estadual de Campinas, UNICAMP, Campinas-SP, Brazil

^fUniversidade Estadual de Feira de Santana, UEFS, Feira de Santana-BA, Brazil

^gUniversidade Federal da Bahia, UFBA, Salvador-BA, Brazil

^hUniversidade Federal do Oeste da Bahia, UFOB, Barra-BA, Brazil

Abstract

We present the status of the Angra Neutrino Experiment, aimed at developing an antineutrino detector for monitoring nuclear reactor activity. The detector comprises a 1.42 m³ Gadolinium-Water Cerenkov target, surrounded by 50 cm of water shielding, placed inside a commercial container about 30 m from the reactor core, at the Angra II nuclear power plant, Brazil. The 4 GW thermal power of the Angra II reactor will provide a few thousand antineutrino interactions per day. The main challenge of the experiment is to overcome the very high cosmic ray induced background at sea level. The present text describes the construction status and simulations results.

Keywords: Neutrino Detectors, Nuclear Safeguards

1. Introduction

Nuclear reactors are a intense source of antineutrinos and the thermal power released in the fission process is directly related to the emitted antineutrino flux. As antineutrinos interact only weakly with matter and escape the reactor containment without any significant change, measuring the antineutrino flux nearby can provide quasi real time information on the reactor status (on/off) and thermal power, as it has been shown by classical references [1, 2, 3, 4] and also in more recent ones [5, 6]. This unique characteristic makes such de-

tectors a powerful candidate to become in the near future a new tool for monitoring reactor facilities under the regime of nuclear safeguards.

As in all other neutrino experiment, the primary difficulty of the Angra Neutrinos Experiment [7] is the distinction of a small neutrino interaction signal from huge backgrounds from different sources, notably electronics and PMT dark noise, gamma rays from nearby radioactive materials and cosmic rays. The applied use of neutrino detectors on nuclear safeguards requires sea-level operation with minimum material overburden. The development of both electronics and simulations are aimed to accomplish this goal.

In what follows, the detector and electronics design (Sec. 2 and 3) and the simulation latest results (Sec. 4)

*Corresponding author

Email address: janjos@cbpf.br (J. C. Anjos)

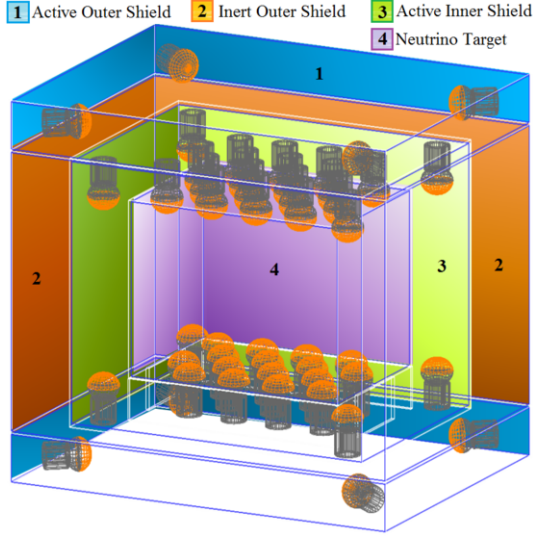


Figure 1: Geometry design of the Angra detector, as modeled with Geant4.

will be described.

2. Detector Design

The adopted detector design is an assembly of four subsystems, here labeled from the outside inwards: (1) two horizontal 25 cm layers (at the top and at the bottom) filled with pure water, equipped with 4 PMTs, acting as active external vetoes; (2) a lateral 25 cm passive water shield that, together with (1), protect the inner parts from cosmic ray induced neutrons and low energy external background as natural radioactivity; (3) a 25 cm intermediate layer of pure water equipped with PMTs, acting as an inner active shield; (4) the neutrino target, based on the water Cerenkov technique, with 0.3 % Gadolinium to enhance neutron capture. Each volume is represented in Fig. 1 as a Geant4 model (more details about the geometry and materials on Sec. 4.2).

Neutrino detection will occur by inverse-beta decay ($\bar{\nu}_e + p^+ \rightarrow n^0 + e^+$), where the emitted positron is above the Cerenkov threshold, thus been visible to the PMTs as a prompt signal. After thermalization, the emitted neutron is captured by the Gd which in turn emits a gamma cascade with average total energy of 8 MeV. These gammas are able to knock out some electrons above the Cerenkov limit, also visible to the PMTs as a delayed signal. The method for neutrino counting relies on the understanding of the temporal correlation between these two signals.

3. Readout Electronics

The readout electronics is composed of a front-end circuit [8, 9] and an acquisition module [10], both developed by the Angra Collaboration. The main functionalities of the former are to read and to conform the PMT signals according to the project requirements while the latter is designed to digitalize and to measure the arriving time of the front-end output signal and to transfer data to a local computer.

3.1. Front-end Module

Eight front-end modules have been produced to fully-equip the detector. Each module has eight channels composed of an Amplifier-Shaper-Discriminator (ASD) circuit; its analog part is shown in Fig. 2. Additionally, each single channel contains an I²C-based circuit able to fine-tune the discriminator thresholds and the offset of the output signals.

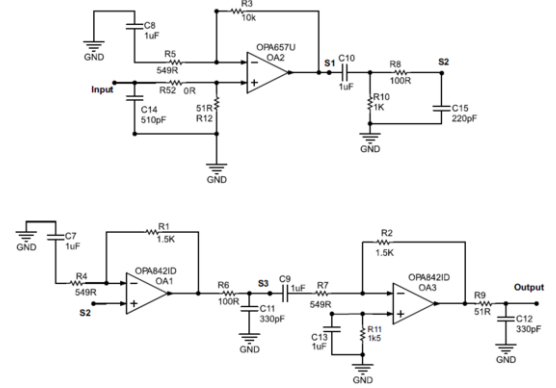


Figure 2: Neutrinos-Angra front-end analog circuit.

The ASD circuit has been characterized for three different gains. The relations between the input charge and the output peak amplitude are shown in Fig. 3 where the circuit linearity and the saturation region can be observed. Considering the highest gain configuration (*Gain-A*), the ASD circuit is linear up to a charge of 60 pC, which corresponds to approximately 37 single-photoelectrons, taking into account a PMT gain of 10^7 . For the lowest gain configuration (*Gain-C*), this value arrives to about 100 photoelectrons.

Fig. 4 shows the average waveforms in response to single photoelectrons for the three tested gain configurations. The front-end output signal has a peak time of 48 ns and a full width at half maximum (FWHM) of 74 ns.

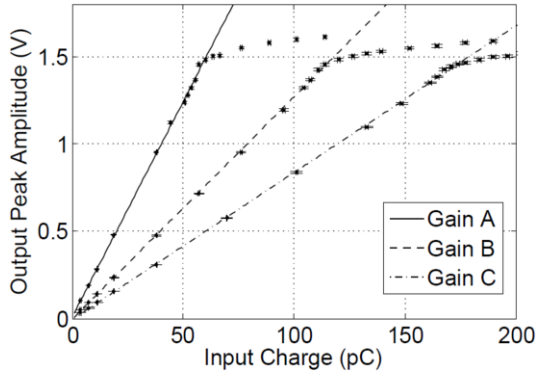


Figure 3: Front-end input charge versus output peak amplitude measurement for three different gains.

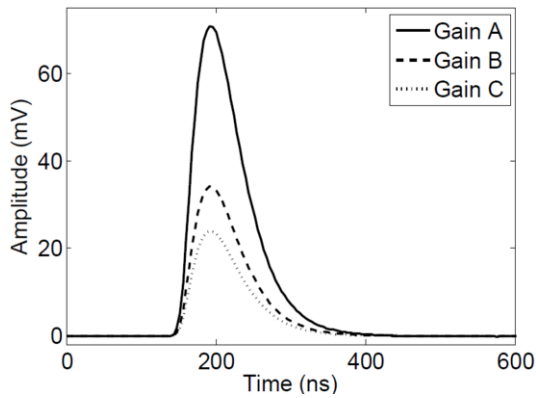


Figure 4: Front-end average waveforms in response to single photo-electrons for three different gains.

3.2. Acquisition Module

The Neutrino DAQ: Each analog-to-digital conversion channel is implemented using a 12-bit multi-stage pipeline ADC able to sample the input signal at 125 MHz. With resolution of 10 bits and a dynamic range of 2 Vpp, a voltage resolution around 2 mV is achieved, which covers the required energy resolution in the detector (considering 4 mV per p.e.). For high-precision time measurement of time between pulses an 8-channel Time-to-Digital Converter integrated circuit has been selected. The TDC presents a resolution of 81 ps and is able to measure pulses in a range of 8 μ s. ADC and TDC information converge at the FPGA core, which build both measurements together for further readout by the control software through the VME bus. The low-level readout software runs on a commercial Single Board Computer under Debian OS.

4. Simulations

The simulations are required to describe properly the interaction between the primary sources (neutrinos or backgrounds) and the detector, reproduce the correct distribution of photo-electrons generated in each PMT for each kind of interaction (both in number and in timing), estimate frequencies of single interaction and of coincidences assuming Poisson statistics for all the primary sources, estimate the signal over noise for the neutrino detection and the capability to reconstruct the actual number of neutrino interactions in realistic conditions. For this reason the software is divided into logical units which interact through well defined interfaces.

4.1. Primary Generators

The fundamental quantity of interest for each kind of primary source is the differential directional intensity[2] (the number of particles dN incident on an area dA in a unit of time dt , per unit of energy dE within a solid angle $d\Omega$):

$$I_i(E, \theta, \phi) = \frac{dN_i}{d\Omega dE dt dA} \quad (1)$$

where i is the primary particle species and θ and ϕ the incoming direction. *A priori*, the intensity may depend on the position within the detector. We consider however an initial primary intensity homogeneous over a volume encompassing the full detector. As the interaction between primaries and detector materials will shield inner detector parts from many backgrounds, it is necessary to consider both angular and energy distributions for each particle species. Proper integrals of differential intensities permit the calculation of fluxes and rates.

4.1.1. Neutrino interactions

A reasonable approximation of the neutrino interaction rate in a water can be calculated according to:

$$R_v = \frac{N_f N_p \langle \sigma \rangle}{4\pi D^2} \quad (2)$$

where N_f is the average fission rate, given by:

$$N_f = 6.24 \times 10^{-8} \left(\frac{P_{th}}{\text{MW}^{-1}} \right) \left(\frac{\text{MeV}}{W} \right) s^{-1} \quad (3)$$

and $P_{th} \approx 4 \times 10^3$ MW is the nominal reactor thermal power, $W = 203.78$ MeV is the average energy release per fission, $\langle \sigma \rangle = 5.825 \times 10^{-43} \text{ cm}^2$ is the average cross section, N_p is the number of protons in the fiducial

Particle	Intensity	Particle	Intensity
Electrons	4.4×10^{-3}	Pions	6.32×10^{-6}
Positrons	1.7×10^{-3}	Protons	1.87×10^{-4}
Photons	1.27×10^{-2}	Neutrons	3.6×10^{-3}
Muons	8.0×10^{-3}		

Table 1: Cosmic ray intensities per particle species. Values correspond to total intensities [$\text{s}^{-1}\text{sr}^{-1}\text{cm}^{-2}$] (Ref. [13])

volume and $D \approx 30$ m is the core-detector distance. For a water target (H_2O), this equation reduces to

$$R_v \approx 3.215 \times 10^6 \left(\frac{V}{\text{m}^3} \right) \left(\frac{\text{m}}{D} \right)^2 \text{ events/day} \quad (4)$$

Considering a fiducial volume $V \approx 1.42 \text{ m}^3$ we get $R_v \approx 5.07 \times 10^3 \text{ events/day}$. This estimate is good enough for the present studies and more refined rate calculations, including the reactor core isotopic evolution and other effects, as shown in [11], will be performed later on at the analysis stage. Anti-neutrino interactions via inverse beta decay result in the production of a positron and a neutron. The simulation of the direction and energy distributions of these two products is modeled according to reference [12], where a detailed description of the differential cross-sections is presented. The neutrino intensity is considered uniform through all the detector.

4.1.2. Cosmic rays

A compilation of cosmic ray intensities for various particle species (electrons, muons, neutrons, photons, pions, positrons and protons) have been collected from references [13, 14]. For a given species i , we consider differential intensities of the form: $I_i(E, \theta, \phi) = I_{vi}(E) \cos^2 \theta$, with vertical intensities $I_{vi} \equiv I_i(\theta = 0)$. The total intensities used are shown in Tab 1. In order to simulate a uniform intensity through the detector volume we first draw a particle direction and then choose its starting position on a surface $5 \times 5 \text{ m}^2$, orthogonal to the direction. The surface is at 4 m from the center of the detector. Finally, the particle energy (or momentum) is chosen according to the vertical intensity. In this way, incoming direction and initial energy are considered as independent variables: a more refined simulation, including correlations, will be implemented if necessary.

4.1.3. Gamma rays from the environment

The intensity of gamma rays from surrounding materials is considered isotropic and its spectrum have been measured by a High-Resolution Germanium detector [15]. The total intensity is normalized to about

$16 \text{ photons s}^{-1}\text{cm}^{-2}$. Only a small fraction of these photons, however, is able to produce an electron (by Compton scattering for example) with speed above the Cerenkov threshold.

4.1.4. Calibration Source

Future calibration of the neutron capture and gamma yield will be performed using a known Californium source (Cf^{252}). Simulation of this neutron source is needed with the purpose of future comparison with the calibration data. The average number of neutrons per fission is known to be $\bar{n} = (3.86 \pm 0.07)$, with a probability P_n of emitting n neutrons on a random fission, implicitly given by [16]:

$$\sum_{i=0}^n P_n = (2\pi)^{-1/2} \int_{-\infty}^{(n+\bar{n}+1/2)/\sigma} \exp(-t^2/2) dt \quad (5)$$

where $\sigma = (1.207 \pm 0.012)$. The energy spectrum of the neutrons is given by an empirical relation

$$\frac{dN}{dE} = \exp\left(-0.88 \frac{E}{\text{MeV}}\right) \sinh\left(2.0 \frac{E}{\text{MeV}}\right)^{1/2} \quad (6)$$

4.2. Geant4 Simulation

Using Geant4 toolbox, the design is based on a clear separation between data specific to the experimental conditions (defined externally) and the actual simulation code. This enables data to be varied according to the known (or hypothetical) errors, in order to estimate the actual experimental errors in the neutrino measurements. The code permits to save with great details intermediate simulation results related to tracks, steps, trajectories and hits, as well as primary particles and vertices. This can be tuned according to the specific analysis. The primary particles are either taken as input either by the HepEvt interface [17] (coming from the primary generators previously described) or created in run time by simpler point-like generators. Hits are divided into two types: PMTHit, representing photoelectrons on the 8" Hamamatsu R5912 PMT, and VetoHit, representing energy released in the veto scintillator. The scintillator veto system however is foreseen to be installed only in a second stage of the experiment and therefore is not simulated at present.

4.2.1. Geometry and Materials

A lot of effort has been invested on the geometrical modeling of the experimental equipment (Fig. 1). The model encompasses the description of several volumes: the target, filled with a solution of water and Gadolinium at 99.7 and 0.3 % mass concentration respectively

(neglecting the presence of Chlorine for the moment), the inner veto, water shield and the top and bottom active shields, all filled with pure water. All the volumes are enclosed by plastic and metallic containers of variable thickness designed to sustain the detector weight, to maintain water purity and to ensure adequate light-tightness. The target is instrumented with 32, 8" PMTs, the inner veto by 8, and the shields by 4 each. The interior surfaces of the active volumes (target, inner veto and active shields) are covered with a white material (Gore in the target and Tyvek elsewhere) to diffuse light with $> 95\%$ efficiency, increasing the overall PMT light collection efficiency. The other two key optical properties are the water absorption length and the PMT quantum efficiency, the first is typical of filtered water, while the second is modeled according to the manufacture's specifications (Hamamatsu). As the water absorption length increases with water purity, and the power plant has an abundant source of ultra-pure water, the total light collection efficiency is modeled in the simulation conservatively.

4.3. Signal and background characterization

After the transport of the primary particles through the detector, we are now able to analyze the shape and distribution of the signals left in the detector.

Charged particles with speed above the Cerenkov threshold emit photons which can be detected by PMTs. Photon collection happens on a time scale of about 10 ns and the front-end electronics have a shaping time of about 100 ns. Moreover, the DAQ electronics (with 8 ns sampling time) acquires a number of samples before the actual start of a signal in order to check the quality of the baseline. All p.e. generated within 512 ns (64 DAQ samples) will therefore appear as a single pulse (we use the word "pulse" to refer to signals in coincidence within this time window). As each PMT has dark noise of about 5 kHz, we expect a global dark-noise in the central detector of about 160 kHz. In order to reduce the trigger rate to acceptable levels it is therefore necessary at least to ask for the coincidence of few p.e. within the 512 ns DAQ time window. For example, asking for at least 5 p.e. in coincidence (using the approximation $R_{\text{coin}} \approx R_{\text{sing}}^n \Delta T^{(n-1)}$ with R_{coin} the desired coincidence rate, R_{sing} the singles rate, and ΔT the coincidence time and n the number of p.e. in coincidence) we expect a dark-noise rate of the order of 10 Hz. With this requirement the dark-noise rate is far below background rates due to other sources. The inverse beta decay interaction results in a positron and a neutron. The positron may have a speed above the Cerenkov threshold and may be directly detected. The two gammas gen-

erated by positron annihilation have an energy of order 0.511 MeV and are unlikely to interact with other electrons to produce Cerenkov light. On the other end, the neutron thermalizes and is absorbed by the Gd, which in turn emits gammas with total energy of about 8 MeV. This gammas may interact with other electrons to produce Cerenkov light.

Analyzing only the events one by one, before the mixing process, it is possible to plan some selection rules (or cuts) to optimize the signal-to-noise ratio. Two selection rules are particularly promising: selecting only events that produce between 10 and 200 p.e. leaves about 90 % positrons and 89 % of neutrons untouched, while reducing dramatically the background level. Further restricting the selection to the interval 20 to 150 p.e., the efficiency drops to 78 % for positrons and 82 % for neutrons. These selection will from now on be referred as *Selection1* and *Selection2*, respectively. The time difference between the prompt (positron) and the delayed (neutron) signals is shown in Fig. 5. We see that 99 % of the events (here we use the word "event" to refer to the coincidence of two pulses) have time interval $\Delta T < 50 \mu\text{s}$ (*TimeSelection1*). One can also see that events with time difference inferior to $5 \mu\text{s}$ are also less likely to occur, which leads another possible time selection rule for events that have time intervals in the range $5 \mu\text{s} \leq \Delta T \leq 50 \mu\text{s}$ (*TimeSelection2*). This selection rule results in an efficiency of about 89 %. Although more stringent on the neutrino signal, *TimeSelection2* is ideal to prevent correlated background, when a positron and a neutron from cosmic sources could mimic a neutrino signal. The overall combined efficiency is 79 % for the combined loose selections ($S1 = \text{Selection1} + \text{TimeSelection1}$) and 54 % for the more strict ones ($S2 = \text{Selection2} + \text{TimeSelection2}$). These two combinations will be carried out to the mixer analysis. We therefore expect to select a rate of neutrino interaction of about 4.0 k events/day with *S1* and 2.7 k events/day with *S2*. Due to the mixing process, the final efficiencies have a tendency to be slightly lower.

Some remarks and highlights from the simulation are in order. It has been observed from the simulations that the relation between the number of p.e. in the prompt pulse and positron momentum may be regarded as been linear, for the purpose of measuring the emitted neutrino flux as a function of the reactor's burn-up. Also, pulses with more than 300 p.e. are mainly due to the passage of muons, while pulses with less than that are mainly due to the neutral component of cosmic rays (neutrons and gammas). The total rate is about 1.5 kHz, with about 350 Hz due to muons. Most of the background pulses however are easily vetoed by the external

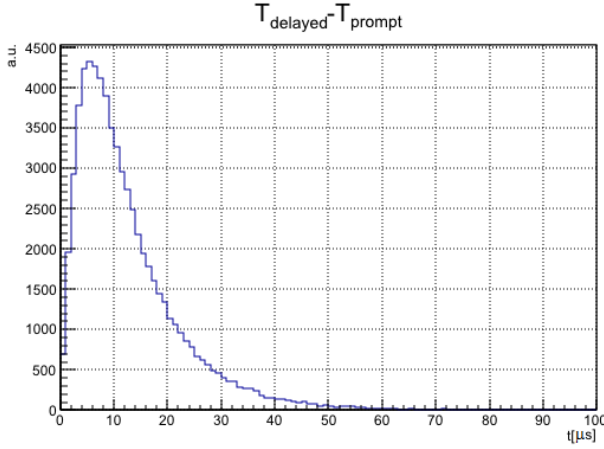


Figure 5: Time difference between prompt and delayed events. The average value around $10\mu\text{s}$ is expected due to the chosen Gd concentration of 0.3 %.

modules, since from those values a total rate of 72 Hz would pass *Selection1* and 56 Hz *Selection2*. The rate of uncorrelated (random) background events passing *S1* is 4.5×10^{-4} Hz and 7.2×10^{-7} Hz for *S2*, both well below the neutrino selection rates (0.047 Hz with *S1* and 0.032 Hz with *S2*). About 20 % of muons generating a signal in the target are followed by at least a second pulse (called secondary) due to different process as muon decay, spallation neutrons etc. Secondary pulses with intervals smaller than about $5\mu\text{s}$ are mostly due to muon decay. Moreover about 18 % of secondaries fulfill *S1* and 14 % *S2*. Assuming that 1 % of primaries are not vetoed, it is expected that the rate of correlated signals due to muons is 0.13 Hz with *S1* and 0.10 Hz with *S2*, both higher than the neutrino signal. It is worth remarking, however, that this background can be measured during reactor off periods and partially (at least the component not involving spallation neutrons) with a pure water target. Assuming a perfect accuracy in the background rate measurement we therefore have a signal-to-noise $S/N \equiv S/\sqrt{BG} = 38$ with *S1* and $S/N = 29$ with *S2* after 24 h of data acquisition. We therefore stress the importance of background measurements for the success of the project.

4.4. Mixer

The Mixer is the piece of software responsible for generating the time distribution for everything that might leave a signal in the detector. It takes as inputs the single events generated by each primary particle (and transported through the detector by Geant4) and a list of frequencies f_i for each primary species. Due to the generation procedure employed for cosmic backgrounds (as

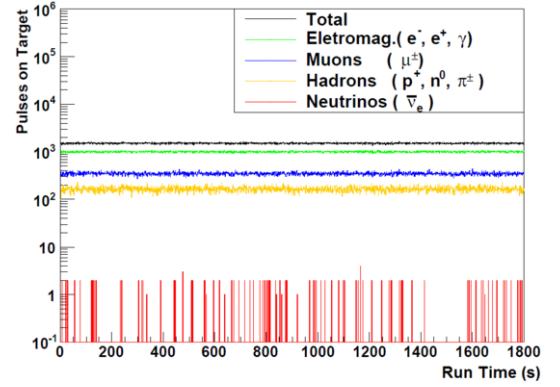


Figure 6: Pulses (p.e. in a 500 ns window) on Target, per second. The black line is the total rate (1.5 kHz on average), while the red represents pulses containing either the prompt or the delayed neutrino signals. Other colors show the EM (green), the muonic (blue) and hadronic (yellow) components of the cosmic background.

previously detailed in Sec. 4.1.2), a number of primaries do not leave any signal on the detector, mainly because of the random directions (also due to shielding efficiency). The frequencies are corrected by the ratio of events that produced any signal (p.e. on PMTs) by the total number of simulated primaries. This leads to an effective frequency \tilde{f}_i for each species. The Mixer then generates a time sequence assuming an exponential distribution. The result is a Poisson process where the average time between particles of the same kind is $\tau_i = 1/\tilde{f}_i$. The output of the mixer is time ordered collection of pulses, mimicking the kind of signal the electronics will face with the real detector. Fig. 6 shows the number of pulses per second on a 3600 s sample, generated on the target volume. The first result of the mixer is the total (background dominated) rate of pulses on the target, which is 1.5 kHz. Section 4.5 will describe how to significantly reduce the background rate, based on study of the mixer's output. A remark on the environmental gammas is in order: due to the 50 cm water shielding, the already small Cerenkov signal generated by this source is strongly suppressed, thus making it a negligible background.

4.5. Signal optimization

For the purpose of validating the selection strategies devised on Sec. 4.3 (namely, *S1* and *S2*) two sets of 24 samples each (simulating 24 h of data taking) were mixed for this study. Each set has the following characteristics: Set 1 contains a mixing of background and antineutrino signal (all sources described in Tab. 1). Events are identified via a MC tag so that each pulse is related to a specific primary event (thus, the type of

source is also identified). Set 2 contains only background events. The two sets can be read as individual packages of 1h, or sequentially up to 24 h of physics with (1) or without (2) the neutrino source, depending on the analysis. The random seeds were different for each hour, so the two sets may be regarded as independent days of data taking.

According to the MC information retained in the mixed data, from the 5 k $\bar{\nu}_e$ expected to be generated, around 4.5 k are fully contained, i.e., both prompt and delayed signals generated pulses inside the target. From Eq. 4, it is possible to obtain the effective volume of $1.26 m^3$ for the target, meaning that if the antineutrino interaction does not happen on a smaller volume inside the target, the event is unlikely to be identified.

The neutrino counting is performed as follows: the first selection rule (*Selection1* or *Selection2*) is applied on the sample, eliminating pulses with p.e. numbers outside the given range. The time difference of the remaining pulses is calculated, generating a histogram in the same manner as Fig. 5. The last step is the application of the second selection rule (*TimeSelection1* or *TimeSelection2*) leaving only values that fall in the predetermined interval. These values constitute neutrino candidates.

Starting with set 1 (signal+BG), strategy *S1* selects 206985 candidates. For the sake of validating the strategy, these values can be split into signal and background using their MC tags, obtaining: $2747\bar{\nu}_e + 201587BG$. While the efficiency prediction from the unmixed sample is 79 %, the corresponding value after the mixer is $61 \pm 1\%$ (uncertainties are statistical only). In order to be able to observe the signal, it is enough that the antineutrino counts are larger than the background fluctuations, rather than the background itself. So the S/N (signal to noise) ratio is $S/\sqrt{BG} = 6.1 \pm 0.2$.

There is a clear discrepancy in both values when compared to the unmixed estimations. This effect might be attributed to the fact that the unmixed analysis looks to the data from an “event” perspective, i.e., the selection strategies remove the entire event while now, after the mixing, selection removes only individual pulses. The end result is that the unmixed expectations always overestimates the amount of signal cut by the selections strategies.

Repeating the process with strategy *S2* leads to $71110 = 1946\bar{\nu}_e + 69164BG$, with efficiency 43 % and S/N ratio of $S/\sqrt{BG} = 7.4 \pm 0.5$. The last value means that although the neutrino counting efficiency is lower, strategy *S2* is actually more effective on preventing the background as the unmixed analysis could reveal.

The next step is to mimic a blind analysis, using set

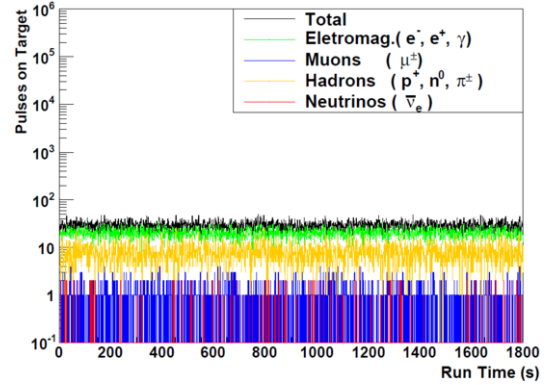


Figure 7: Number of pulses on Target (per second), after applying selection *S1*. The total background rates were cut from 1.5 kHz to 36 Hz. Analyzing the components of the background, it is possible to see that strategy *S1* is in fact very effective on muons (in blue), but less restrictive to other components, like the EM (green) and hadronic (yellow) ones.

2 (background only). By applying strategies *S1* and *S2* to this set, a total of 201597 and 68236 candidates are selected. These can be regarded as a real measure performed with the reactor off (or away from the reactor). Taking into account the statistical fluctuations of these measurements, we have $N_{\text{off}} = BG \pm \sqrt{BG} = (201.6 \pm 0.4) \times 10^3$ counts with *S1* and $(68.2 \pm 0.3) \times 10^3$ with *S2*. Now, consider a measurement done with the same duration (24h) with reactor on, here presented as the set 1. A total count of candidates leads to (from the values previously presented) $N_{\text{on}} = (207.0 \pm 0.4) \times 10^3$ and $(69.2 \pm 0.3) \times 10^3$ for *S1* and *S2*, respectively. So, subtracting the reactor on counts from the reactor off, we have our signal:

$$N_{\bar{\nu}_e}(S1) = (5.4 \pm 0.6) \times 10^3 \quad (7)$$

$$N_{\bar{\nu}_e}(S2) = (9 \pm 4) \times 10^2 \quad (8)$$

Although *S1* resulted on a non zero signal with a significance larger than 5σ , the *S2* strategy demands more statistics. This is the consequence of dealing with large numbers (the total counts) and their Poisson variances. While the S/N ratio was favorable for set 1, the statistical uncertainties related to the Poisson processes are still large for a 24 h run, mainly in the case of choosing the *S2* strategy. For this reason, the particular values obtained in these calculations (Eqs. 7 and 8) cannot be regarded as a absolute prediction of the simulation, but rather as a prove of concept. Taking the efficiencies obtained for set 1 as a reference, it is possible to calculate that a 10 day data set would bring the uncertainties of both strategies to the 5 % level. This may be

taken as an inferior limit for the time needed for Angra to blindly distinguish between the reactor-ON and reactor-OFF situations.

5. Conclusion

The present analysis shows that with appropriate selections it is possible to detect neutrino interactions from the Angra-II power plant with a sea-level Water-Cerenkov detector, with 95% confidence level, after a minimum of 10 days of data acquisition. This is based on the simulations assumptions and the real time will be naturally larger due to the ideal character of these hypothesis and the efficiency of the data acquisition, which was not considered here. Still, simulations are required to be calibrated by real background measurements, which could improve these predictions. These measurements are already being performed at the CBPF site, which will be a first estimate of the expected background at the Angra site.

Acknowledgments

This work is supported by several agencies, through a large number of funding projects. The Angra Collaboration acknowledges the support of Ministério da Ciência, Tecnologia e Inovação (MCTI), the Conselho Nacional para o Desenvolvimento Científico e Tecnológico (CNPq), Financiadora de Estudos e Projetos (FINEP) and the following state research agencies: FAPESP, FAPEMIG and FAPERJ. We also thank Dr. T.J.C. Bezerra and A. Cabrera for fruitful discussions and comments.

References

- [1] A. A. Borovi, L. A. Mikaelyan, Possibilities of the practical use of neutrinos, *Soviet Atomic Energy* 44 (1978) 589–592. doi:10.1007/BF01117861.
- [2] V. A. Korovkin, et al., Remote monitoring of reactor by means of neutrino instrument in process room of rovnoe nuclear power plant, *Soviet Atomic Energy* 71 (1991) 1018–1022.
- [3] A. Bernstein, Y. Wang, G. Gratta, T. West, Nuclear reactor safeguards and monitoring with antineutrino detectors, *Journal of Applied Physics* 91 (2002) 4672–4676. arXiv:0108001, doi:10.1063/1.1452775.
- [4] A. Bernstein, N. S. Bowden, A. Misner, T. Palmer, Monitoring the thermal power of nuclear reactors with a prototype cubic meter antineutrino detector, *Journal of Applied Physics* 103. arXiv:0804.4723, doi:10.1063/1.2899178.
- [5] N. S. Bowden, Reactor monitoring using antineutrino detectors, *Nuclear Physics B - Proceedings Supplements* 217 (2011) 134–136. arXiv:0809.2128, doi:10.1016/j.nuclphysbps.2011.04.085.
- [6] T. Classen, A. Bernstein, N. S. Bowden, B. Cabrera-Palmer, A. Hoc, G. Jonkmans, L. Kogler, D. Reyna, B. Sur, Development of an advanced antineutrino detector for reactor monitoring, *Physics Research A* 771 (2014) 139–146. doi:10.1016/j.nima.2014.10.022.
- [7] J. Anjos, A. Barbosa, R. Funchal, E. Kemp, J. Magnin, H. Nunokawa, O. Peres, D. Reyna, R. Shellard, Angra Neutrino Project: status and plans, *Nuclear Physics B - Proceedings Supplements* 155 (1) (2006) 231–232. doi:10.1016/j.nuclphysbps.2006.02.058.
- [8] J. A. Costa, Eletrônica de front-end do experimento neutrinos-angra, Master's thesis, UFJF (2014).
- [9] T. I. Dornelas, Medidas de caracterização do sensor, da eletrônica de leitura e do detector alvo do projeto neutrinos-angra, Master's thesis, UFJF (2015).
- [10] H. P. Lima, Data acquisition system for the angra project - angra note 12, Tech. rep., Angra Collaboration (2009).
- [11] Y. Abe, et al., Reactor ν_e disappearance in the double chooz experiment, *Phys. Rev. D* 86 (2012) 052008.
- [12] P. Voguel, J. F. Beacom, Angular distribution of neutron inverse beta decay, $\nu_e + p \rightarrow e^+ + n$, *Phys. Rev. D* 60 (1999) 053003.
- [13] P. K. F. Grieder (Ed.), *Cosmic Rays at Earth*, Elsevier Science, 2001.
- [14] Measurement and reporting of alpha particle and terrestrial cosmic ray-induced soft errors in semiconductor devices (2012).
- [15] T. Abrahao, Detecção de antineutrinos de reatores e medidas de fontes de ruído, Master's thesis, CBPF (2012).
- [16] J. Terrell, Distributions of fission neutron numbers, *Physical Review* 108 (1957) 783–789.
- [17] L. Garren, P. Lebrun, *StdHep 5.06.01 - Monte Carlo Standardization at FNAL* (2006). URL <http://cepa.fnal.gov/psm/stdhep/>